Volume 60 Issue 3 March 2012 ISSN 0022-5096

ELSEVIER

JOURNAL OF THE
MECHANICS AND PHYSICS
OF SOLIDS

Journal of the Mechanics and Physics of Solids 60 (2012) 418–431

Contents lists available at SciVerse ScienceDirect

Journal of the Mechanics and Physics of Solids

journal homepage: www.elsevier.com/locate/jmps

Elastic fields of dislocation loops in three-dimensional anisotropic bimaterials

H.J. Chu [a,b,d], E. Pan [b], X. Han [c], J. Wang [d,*], I.J. Beyerlein [e]

[a] Research Group of Mechanics, Yanzhou University, Yangzhou 225009, China
[b] Department of Civil Engineering, University of Akron, Akron, OH 44325, USA
[c] Department of Mechanics, Beijing Institute of Technology, Beijing 1000081, China
[d] Materials Science and Technology Division, Los Alamos National Laboratory, Los Alamos, NM 87545, USA
[e] Theoretical Division, Los Alamos National Laboratory, Los Alamos, NM 87545, USA

ARTICLE INFO

Article history:
Received 25 March 2011
Received in revised form
1 December 2011
Accepted 13 December 2011
Available online 23 December 2011

Keywords:
Dislocation loop
Line integral
Green's function
Bimaterial interface

ABSTRACT

By applying semi-analytical point-force Green's functions obtained via the Stroh formulism, we derive simple line integrals to calculate the elastic displacement and stress fields for a three-dimensional dislocation loop in an anisotropic bimaterial system. The solutions for the case of anisotropy are more convenient for treating an arbitrary dislocation loop compared with traditional area integration. With this new formulation, we numerically examine the displacement, stress, and energy due to the interaction between a dislocation loop and the bimaterial interface in an Al–Cu system. The interactive image energy due to the elastic moduli mismatch across the interface is then numerically evaluated. The result shows that a dislocation loop is subjected to an attractive force by the interface when it lies in the stiff material, and a repulsive force when it lies in the soft material. Moreover, the dependence of the interactive image energy of a dislocation loop on the position and size of the dislocation loop are also demonstrated and discussed. Significantly, it is found that the interactive image energy for a dislocation loop depends only on the ratio d/a, where a is the loop diameter and d is its distance to the interface. The examples studied provide benchmark solutions for anisotropic bimaterial dislocation problems.

Published by Elsevier Ltd.

1. Introduction

Stress fields that arise due to the presence of an elastic modulus mismatch across a bimaterial interface are fundamental to understanding the nature of dislocation/interface interactions in two-phase composites. An approaching dislocation perturbs the stress field on the interface, while in turn, the discontinuity in material stiffness across the interface alters the stress field on the dislocation. Their interaction can result in blocking, transmission, or absorption of the dislocation by the interface (Demkowicz et al., 2008; Lu et al., 2009; Wang et al., 2008a,b, 2011). The significance of such defect/interface interactions increases when the composite material contains an unusually high density of interfaces, such as in multi-layered nanocomposites (Misra, 2008; Mara et al., 2008, 2010; Han et al., 2011). For this particular lamellar architecture, defect–interface interactions have been studied extensively from the atomistic to dislocation scale (Freund, 1990; Anderson et al., 1999; Ghoneim and Han, 2005; Akasheh et al., 2007a,b; Demkowicz et al., 2008;

* Corresponding author. Tel.: +1 505 667 1238.
E-mail address: wangj6@lanl.gov (J. Wang).

0022-5096/$ - see front matter Published by Elsevier Ltd.
doi:10.1016/j.jmps.2011.12.007

Wang et al., 2009a,b; Wang and Misra, 2011; Zhang et al., 2011). Altering the layer thickness within the submicron to nanoscale regime causes dramatic changes not only in the overall strength of the composite, but also in the nature of the defect/interface interactions (Misra and Kung, 2001; Misra et al., 1999, 2002). For layer thicknesses greater than ≈ 50–100 nm, dislocations tend to pile-up leading to a Hall-Petch scaling law for strength. As the layer thickness reduces to a few tens of nanometers, the dislocations are confined by two neighboring interfaces to expand within the layer, a mechanism called confined layer slip. For layers less than 10 nm, the latter mechanism becomes less favorable compared to dislocation transmission across the interface. The processes of transmission or nucleation involve dislocation loops of a number of possible orientations and sizes closely interacting with the interface. Atomic-scale simulations of defect/interface interactions necessarily only consider a few specific cases. A more general analytical approach to this problem would help advance a deeper understanding and provide insight into some of the observations from simulations.

Towards this end, in this work, we study the energetics and mechanics of dislocation loops of arbitrary size and position within an anisotropic bimaterial, containing a single interface. To accomplish this task, we derive line-integral expressions for the elastic fields induced by an arbitrary shaped dislocation loop in an anisotropic bimaterial system. The major challenge here involves reducing the surface integral to a line integral for the displacement and stress fields associated with the image part in the case of elastic anisotropy since Stokes' theorem cannot be utilized.

Theoretical analyses based on Green's function techniques have been successful in providing analytical solutions for the elastic displacement and stress fields produced by dislocations. Fundamentally, these elastic fields can be expressed as an integral of a point-force Green's function and its derivatives over the dislocation surface (Volterra, 1907; Mura, 1963; Willis, 1970; Hirth and Lothe, 1982; Wang, 1996; Han and Ghoniem, 2005). For homogeneous materials, this method has been applied directly to calculate the elastic fields (Mura, 1987). For heterogeneous (bi- or multi-layered) materials, the point-force Green's function is often divided into two terms: the full-space term and image term (Fares and Li, 1988; Ting, 1996; Pan and Yuan, 2000). The full-space term corresponds to the point-force Green's function in a homogenous material encompassing the entire space, and the image one is induced by image point forces that arise from the elastic mismatch across interfaces. Accordingly, the elastic field of a dislocation in the bimaterial can be separated into two parts associated with the two point-force Green's functions (Akarapu and Zbib, 2009). Generally, both parts can be evaluated by surface integrals.

By applying the Stokes' theorem, the surface integral of the strain/stress field of a dislocation loop in a full space can be reduced to the integral along the dislocation line (Mura, 1963). For anisotropic materials, the analytical expression of the stress/strain field due to a straight segment of a dislocation loop in an anisotropic solid was derived by Willis (1970) and Wang (1996). Recently, Chu et al. (2011) obtained a line-integral expression of the elastic displacement for dislocation loops in a 3D anisotropic full space. Comninou and Dundurs (1975) obtained an analytical expression for the stress field generated by an angular dislocation in an isotropic half space. Ben-Zion (1990) studied the elastic response of two isotropic half spaces to point dislocations at their common interface. Yu and Sanday (1991) presented a line integral solution for a circular dislocation in an isotropic bimaterial system. Gosling and Willis (1994) derived a line integral for the stresses associated with an arbitrary dislocation in an isotropic half-space. Ghoniem and Han (2005) proposed a line-integral expression (along the dislocation boundary) for the elastic fields produced by dislocations in multilayered materials of elastic anisotropy. Since their integrand (i.e., the point-force Green's function) includes a line integral from 0 to π, their solution involves a double integral. Akarapu and Zbib (2009) recently constructed line-integral expressions for the displacement and stress fields associated with an arbitrary shaped dislocation in an isotropic bimaterial. These line-integral expressions were used in their computational dislocation dynamic codes to enhance the computation efficiency in calculating stress fields. On the other hand, singularity on/around the dislocation loops is a long-standing issue (Chu et al., 2011). Several models have been proposed to overcome it. For instance, to avoid the singularity that would be produced from linear elastic dislocation theory, Cai et al. (2006) proposed a non-singular continuum theory of dislocations. Fitzgerald and Aubry (2010) assumed that the core energy follows a similar form to the elastic energy. Gavazza and Barnett (1976) separated the total energy into the core energy (in their words the "tube-part") and the elastic part (the "cut-part") lying outside of the tube. The core energy is then evaluated using the Stroh's vector Airy stress function for an infinite straight dislocation, which is a two-dimensional problem. Hirth and Lothe (1982) suggested choosing a cut-off value small enough to make the contribution of the core when carrying out integration of the elastic strain energy. In this case a suitable "cut-off" radius for the core region ranges from $0.5b$ to $2b$ (with b being the magnitude of the Burgers vector). It is worth pointing out the exact value for the cut-off for a specific case can only be determined via atomistic simulations, which varies with dislocation type and interatomic potential. Thus, physically, the results in the core region obtained by continuum mechanics are not useful.

The present work continues beyond previous work in this area by treating a bimaterial interface formed by two elastically anisotropic crystals. These calculations are accomplished by a line integral formulation that we develop in this work. This formulation can efficiently and accurately calculate the elastic displacement, strain, and stress fields due to a loop of any size and shape located near a bimaterial interface in a three-dimensional (3D) space. The theory allows for any arbitrary orientation relationship and relative position in space between the loop and interface. Most materials of interest are elastically anisotropic, and hence it is of considerable importance to account for the mismatch in the anisotropic stiffness tensor across the bimaterial interface when calculating these elastic fields.

This paper is organized as follows. In Section 2, we present general integral expressions for the elastic fields produced by a dislocation loop located in an elastically anisotropic half space bonded to the other half space with different anisotropic elastic properties. The section ends with the solutions for the image displacement and strain. In Section 3, we implement the proposed approach to study the displacement and stress fields that a dislocation produces on the interface and the variation in the interactive image energy with the size a and position d of the dislocation loop from the interface. It is found that the interactive image energy for a dislocation loop depends only on the ratio d/a. Conclusions are drawn in Section 4.

2. Integral expressions of elastic fields in anisotropic elastic bimaterials

The problem of interest consists of a dislocation loop in a crystal joined to another with dissimilar anisotropic elastic properties. The jump in elastic moduli across the interface perturbs the elastic displacement, strain, and stress distributions in the material. The line integral formulation developed here provides the solution for these fields as a function of the dislocation position, character, strength (Burgers vector), and geometry.

We consider a general dislocation surface denoted by S located in the upper half space ($x_3>0$) in an anisotropic bimaterial space. The upper surface of the dislocation denoted by S^+ slips by the Burgers vector $\boldsymbol{b}$ relative to the lower surface denoted by S^-. The normal vectors of the upper and lower surfaces are $\boldsymbol{n}^+$ and $\boldsymbol{n}^-$, respectively.

2.1. The displacement and strain fields for a dislocation loop

The constitutive relation for a material of general elastic anisotropy is given by

$$\sigma_{ij}=C_{ijkl}\varepsilon_{kl} \tag{1}$$

In this paper, repeated indices obey the summation convention from 1 to 3, unless noted otherwise. Following the work by Volterra (1907), Mura (1963), Gosling and Willis (1994), Pan (1991), and Han and Ghoniem (2005), the elastic displacement induced by the dislocation S is

$$u_k(\boldsymbol{y})=\int_S C_{ijml}(\boldsymbol{x})G_{mk,x_l}(\boldsymbol{y};\boldsymbol{x})b_j(\boldsymbol{x})n_i(\boldsymbol{x})\mathrm{d}S(\boldsymbol{x}) \tag{2}$$

where $G_{mk}(\boldsymbol{y};\boldsymbol{x})$ is the point-force Green's function representing the elastic displacement in the m-direction at $\boldsymbol{x}$ induced by a point force in k-direction applied at $\boldsymbol{y}$; $n_i=n_i^-$ denotes the cosine of the normal unit vector of the dislocation surface; b_j is the jth component of the Burgers vector. From Eq. (2), the displacement gradient can easily be obtained as:

$$u_{k,p}(\boldsymbol{y})=\int_S C_{ijml}(\boldsymbol{x})G_{mk,x_ly_p}(\boldsymbol{y};\boldsymbol{x})b_j(\boldsymbol{x})n_i(\boldsymbol{x})\mathrm{d}S(\boldsymbol{x}) \tag{3}$$

Here we emphasize that, if the dislocation is located in an isotropic and homogeneous full space, Eq. (3) can exactly be reduced to a line integral as given by Mura (1963), and Gosling and Willis (1970). In the bimaterial case, since the Green's function does not satisfy the derivative relationship $\partial G(y,x)/\partial x=-\partial G(y,x)/\partial y$, it is difficult to convert the involved surface integral into a line integral.

2.2. Point-force Green's function for bimaterials

Integration of Eqs. (2) and (3) over the dislocation surface requires the point-force Green's function. The study of Green's function for an anisotropic half-space or a bimaterial system can be traced back to the work of Mindlin (1936) and Barnett and Lothe (1974). The Green's functions for an anisotropic bimaterial system were obtained by Pan and Yuan (2000) via the Stroh formalism and Fourier transform, and their results are briefly reviewed below for the sake of completeness.

We first introduce the Stroh eigen equation for an anisotropic material, which is (Ting, 1996)

$$[\mathbf{Q}+p(\mathbf{R}+\mathbf{R}^T)+p^2\mathbf{T}]\boldsymbol{a}=0 \tag{4}$$

with

$$\begin{aligned}&Q_{ij}=C_{ikjs}n_kn_s,\quad R_{ij}=C_{ikjs}n_km_s,\quad T_{ij}=C_{ikjs}m_km_s\\&\boldsymbol{n}=[\cos\theta,\sin\theta,0]^T,\quad \boldsymbol{m}=[0,0,1]^T\end{aligned} \tag{5}$$

where the superscript 'T' denotes the transpose of the matrix. In Eq. (4), p_i, and $\boldsymbol{a}_i$ ($i=1$, 2, 3) are the eigenvalues and the associated eigenvectors, respectively. We further define

$$\begin{aligned}&\mathrm{Im}(p_i)>0,\ \ p_{i+3}=\overline{p}_i,\ \ \overline{\boldsymbol{a}}_{i+3}=\overline{\boldsymbol{a}}_i,\quad (i=1,2,3)\\&\mathbf{A}\equiv[\boldsymbol{a}_1,\boldsymbol{a}_2,\boldsymbol{a}_3],\ \ \mathbf{B}\equiv[\boldsymbol{b}_1,\boldsymbol{b}_2,\boldsymbol{b}_3]\ \text{ with }\ \boldsymbol{b}_i\equiv(\mathbf{R}^T+p_i\mathbf{T})\boldsymbol{a}_i\end{aligned} \tag{6}$$

where the symbol 'Im' and the overbar denote the imaginary part and the complex conjugate, respectively. There is no summation on the repeated index i in the last expression.

The Green's function (displacement) tensor at field point $\boldsymbol{x}$ in the upper half-space ($x_3>0$) of an anisotropic bimaterial due to a point force at $\boldsymbol{y}$ is

$$\mathbf{G}(\boldsymbol{y};\boldsymbol{x})=\begin{cases}\mathbf{G}^{\infty}(\boldsymbol{y};\boldsymbol{x})-\frac{1}{2\pi^2}\int_0^{\pi}\overline{\mathbf{A}}_1\mathbf{G}_{\mathrm{u}}^{(1)}\mathbf{A}_1^T\mathrm{d}\theta & y_3>0\\ -\frac{1}{2\pi^2}\int_0^{\pi}\overline{\mathbf{A}}_1\mathbf{G}_{\mathrm{u}}^{(2)}\overline{\mathbf{A}}_2^T\mathrm{d}\theta & y_3<0\end{cases}\tag{7}$$

where

$$\begin{aligned}
&[\mathbf{G}_u^{(1)}]_{ij}=\frac{[\mathbf{G}_1]_{ij}}{\boldsymbol{h}(\overline{p}_i^{(1)})\boldsymbol{x}-\boldsymbol{h}(p_j^{(1)})\boldsymbol{y}}\\
&[\mathbf{G}_u^{(2)}]_{ij}=\frac{[\mathbf{G}_2]_{ij}}{\boldsymbol{h}(\overline{p}_i^{(1)})\boldsymbol{x}-\boldsymbol{h}(\overline{p}_j^{(2)})\boldsymbol{y}}\\
&\boldsymbol{G}_1=-\overline{\mathbf{A}}_1^{-1}(\overline{\mathbf{M}}_1+\mathbf{M}_2)^{-1}(\mathbf{M}_1-\mathbf{M}_2)\mathbf{A}_1\\
&\mathbf{G}_2=\overline{\mathbf{A}}_1^{-1}(\overline{\mathbf{M}}_1+\mathbf{M}_2)^{-1}(\overline{\mathbf{M}}_2+\mathbf{M}_2)\overline{\mathbf{A}}_2\\
&\boldsymbol{h}(p_*)=[\cos\theta,\sin\theta,p_*]^T\\
&\mathbf{M}_\alpha=-i\mathbf{B}_\alpha\mathbf{A}_\alpha^{-1}\quad(\alpha=1,2)
\end{aligned}\tag{8}$$

In Eq. (7), $\mathbf{G}^{\infty}(\boldsymbol{y};\boldsymbol{x})$ is the corresponding full-space Green's function tensor, which is available in an explicit form (Pan and Yuan, 2000; Tonon et al., 2001). The superscript '(1)' ('(2)') or subscript '1' ('2') attached to the matrices, vectors, and scalars stand for those related to material 1 (2), i.e., in the upper (lower) half-space with $x_3>0$ ($x_3<0$). There is no summation over the repeated indices i and j in Eq. (8).

In Eq. (7) the field point $\boldsymbol{x}$ of the Green's function must be within the upper half space, i.e. $x_3>0$. It allows for the source to be either in the upper half space, i.e. $y_3>0$, or lower half space, $y_3<0$, an extension of the Green's function obtained by Pan and Yuan (2000), which only assumed the former.

The Green's function tensor at field point $\boldsymbol{x}$ in the lower half-space ($x_3<0$) is

$$\mathbf{G}(\boldsymbol{y};\boldsymbol{x})=\begin{cases}\mathbf{G}^{\infty}(\boldsymbol{y};\boldsymbol{x})-\frac{1}{2\pi^2}\int_0^{\pi}\mathbf{A}_2\mathbf{G}_{\mathrm{u}}^{(2)}\overline{\mathbf{A}}_2^T\mathrm{d}\theta & y_3<0\\ -\frac{1}{2\pi^2}\int_0^{\pi}\mathbf{A}_2\mathbf{G}_{\mathrm{u}}^{(1)}\mathbf{A}_1^T\mathrm{d}\theta & y_3>0\end{cases}\tag{9}$$

where the new matrices $\mathbf{G}_u^{(1)}$ and $\mathbf{G}_u^{(2)}$ are defined as

$$\begin{aligned}
&[\mathbf{G}_u^{(1)}]_{ij}=\frac{-[\mathbf{G}_1]_{ij}}{\boldsymbol{h}(p_i^{(2)})\boldsymbol{x}-\boldsymbol{h}(p_j^{(1)})\boldsymbol{y}}\\
&[\mathbf{G}_u^{(2)}]_{ij}=\frac{-[\mathbf{G}_2]_{ij}}{\boldsymbol{h}(p_i^{(2)})\boldsymbol{x}-\boldsymbol{h}(\overline{p}_j^{(2)})\boldsymbol{y}}\\
&\boldsymbol{G}_1=\mathbf{A}_2^{-1}(\overline{\mathbf{M}}_1+\mathbf{M}_2)^{-1}(\mathbf{M}_1+\overline{\mathbf{M}}_1)\mathbf{A}_1\\
&\boldsymbol{G}_2=\mathbf{A}_2^{-1}(\overline{\mathbf{M}}_1+\mathbf{M}_2)^{-1}(\overline{\mathbf{M}}_1-\overline{\mathbf{M}}_2)\overline{\mathbf{A}}_2
\end{aligned}\tag{10}$$

In order to obtain the displacements and strains induced by a dislocation in a bimaterial system, the Green's functions in Eqs. (7) and (9) should be substituted into Eqs. (2) and (3). It is observed from both Eqs. (7) and (9), that the Green's functions can be separated into two parts: one corresponds to the full-space $\mathbf{G}^{\infty}(\boldsymbol{y};\boldsymbol{x})$ and the other includes the remaining terms that are associated with the bimaterial interface. We will refer the latter as the image Green's function. Substituting Eq. (7) into Eqs. (2) and (3) results in the integral over the dislocation surface that we must solve. The first part of the surface integral contains the full-space Green's function. The line-integral expressions for the displacement and stress fields corresponding to this case were recently derived by Chu et al. (2011). Thus, the main task of this work is to solve the second integral that contains the image Green's functions in Eqs. (7) and (9).

2.3. *The line integral expressions for a triangular dislocation*

An arbitrary polygonal shape can be constructed by a finite number of triangles. Accordingly the integral over a polygonal dislocation can be regarded as the summation of the integrals over triangular dislocations. In what follows, we derive the integral expressions of the image part over an arbitrary triangular dislocation in a bimaterial space. With this, we can derive the elastic fields induced by a triangular dislocation, which by the method of superposition, can be utilized to obtain the elastic field due to a polygonal dislocation.

We substitute the image part of Green's function (i.e., the complementary part added to the infinite-space Green's function in order to satisfy the interface condition in the bimaterial space) in Eq. (7) into Eq. (2), and find the image displacement induced by a triangular dislocation, i.e.

$$u_k^{\text{Image}}(\boldsymbol{y}) = \begin{cases} -\frac{1}{2\pi^2}\int_0^{\pi} \mathrm{d}\,\theta \int_\Delta C_{ijml}[\overline{\mathbf{A}}_1 \mathbf{G}_u^{(1)} \mathbf{A}_1^T]_{mk,x_l} b_j n_i \mathrm{d}S(\boldsymbol{x}) & y_3 > 0 \\ -\frac{1}{2\pi^2}\int_0^{\pi} \mathrm{d}\,\theta \int_\Delta C_{ijml}[\mathbf{A}_1 \mathbf{G}_u^{(2)} \mathbf{A}_2^T]_{mk,x_l} b_j n_i \mathrm{d}S(\boldsymbol{x}) & y_3 < 0 \end{cases} \tag{11}$$

Due to the fact that the eigenvector matrices $\mathbf{A}_1$ and $\mathbf{A}_2$, and $\mathbf{G}_1$ and $\mathbf{G}_2$ in Eq. (8) are independent of the field and source points $\boldsymbol{x}$ and $\boldsymbol{y}$, Eq. (11) can be written as

$$u_k^{\text{Image}}(\boldsymbol{y}) = \begin{cases} -\frac{1}{2\pi^2}\int_0^{\pi} \left[C_{ijml} b_j n_i \overline{A}_{1\ mt} A_{1sk}^T \int_\Delta G_{u\ ts,x_l}^{(1)} \mathrm{d}S(\boldsymbol{x})\right] \mathrm{d}\,\theta & y_3 > 0 \\ -\frac{1}{2\pi^2}\int_0^{\pi} \left[C_{ijml} b_j n_i A_{1\ mt} A_{2sk}^T \int_\Delta G_{u\ ts,x_l}^{(2)} \mathrm{d}S(\boldsymbol{x})\right] \mathrm{d}\,\theta & y_3 < 0 \end{cases} \tag{12}$$

Making use of the expression for $\mathbf{G}_u$ in Eq. (8) and with some manipulations, the integral on the triangular dislocation becomes

$$\begin{cases} \int_\Delta G_{u\ ts,x_l}^{(1)} \mathrm{d}S(\boldsymbol{x}) = \int_\Delta \frac{-G_{1ts} h_l(\overline{p}_t^{(1)})}{[\boldsymbol{h}(\overline{p}_t^{(1)})\boldsymbol{x} - \boldsymbol{h}(p_s^{(1)})\boldsymbol{y}]^2} \mathrm{d}S(\boldsymbol{x}) & y_3 > 0 \\ \int_\Delta G_{u\ ts,x_l}^{(2)} \mathrm{d}S(\boldsymbol{x}) = \int_\Delta \frac{-G_{2ts} h_l(p_t^{(1)})}{[\boldsymbol{h}(p_t^{(1)})\boldsymbol{x} - \boldsymbol{h}(p_s^{(2)})\boldsymbol{y}]^2} \mathrm{d}S(\boldsymbol{x}) & y_3 < 0 \end{cases} \tag{13}$$

where the vector $\boldsymbol{h}$ in Eq. (8) has the following components:

$$\begin{aligned} &\boldsymbol{h}(\overline{p}_t^{(1)}) = [\cos\theta, \sin\theta, \overline{p}_t^{(1)}]^T \\ &\boldsymbol{h}(p_t^{(1)}) = [\cos\theta, \sin\theta, p_t^{(1)}]^T \end{aligned} \tag{14}$$

By taking the derivative of the image displacement in Eq. (12), the corresponding image strain can be obtained, which is

$$u_{k,p}^{\text{Image}}(\boldsymbol{y}) = \begin{cases} -\frac{1}{4\pi^2}\int_0^{2\pi} \left[C_{ijml} b_j n_i \overline{A}_{1\ mt} A_{1\ sk}^T \int_\Delta G_{u\ ts,x_l y_p}^{(1)} \mathrm{d}S(\boldsymbol{x})\right] \mathrm{d}\,\theta & y_3 > 0 \\ -\frac{1}{4\pi^2}\int_0^{2\pi} \left[C_{ijml} b_j n_i A_{1\ mt} A_{2\ sk}^T \int_\Delta G_{u\ ts,x_l y_p}^{(2)} \mathrm{d}S(\boldsymbol{x})\right] \mathrm{d}\,\theta & y_3 < 0 \end{cases} \tag{15}$$

The integral over the triangular dislocation in Eq. (15) can be expressed as

$$\begin{cases} \int_\Delta G_{u\ ts,x_l y_p}^{1} \mathrm{d}S(\boldsymbol{x}) = \int_\Delta \frac{-2G_{1ts} h_l(\overline{p}_t^{(1)}) h_p(p_s^{(1)})}{[\boldsymbol{h}(\overline{p}_t^{(1)})\boldsymbol{x} - \boldsymbol{h}(p_s^{(1)})\boldsymbol{y}]^3} \mathrm{d}S(\boldsymbol{x}) & y_3 > 0 \\ \int_\Delta G_{u\,ts,x_l y_p}^{2} \mathrm{d}S(\boldsymbol{x}) = \int_\Delta \frac{-2G_{2ts} h_l(p_t^{(1)}) h_p(p_s^{(2)})}{[\boldsymbol{h}(p_t^{(1)})\boldsymbol{x} - \boldsymbol{h}(p_s^{(2)})\boldsymbol{y}]^3} \mathrm{d}S(\boldsymbol{x}) & y_3 < 0 \end{cases} \tag{16}$$

where by making use of the definition for $\boldsymbol{h}$, we have

$$h_l(\overline{p}_t^{(1)}) h_p(p_s^{(1)}) = \begin{bmatrix} \cos\theta\cos\theta & \cos\theta\sin\theta & \cos\theta p_s^{(1)} \\ \sin\theta\cos\theta & \sin\theta\sin\theta & \sin\theta p_s^{(1)} \\ \overline{p}_t^{(1)}\cos\theta & \overline{p}_t^{(1)}\sin\theta & \overline{p}_t^{(1)} p_s^{(1)} \end{bmatrix} \tag{17}$$

and

$$h_l(p_t^{(1)}) h_p(p_s^{(2)}) = \begin{bmatrix} \cos\theta\cos\theta & \cos\theta\sin\theta & \cos\theta p_s^{(2)} \\ \sin\theta\cos\theta & \sin\theta\sin\theta & \sin\theta p_s^{(2)} \\ p_t^{(1)}\cos\theta & p_t^{(1)}\sin\theta & p_t^{(1)} p_s^{(2)} \end{bmatrix} \tag{18}$$

Since the numerators in the integrands of Eqs. (13) and (16) are independent of $\boldsymbol{x}$, their integrals are related to power functions of $\boldsymbol{x}$ with exponents -2 and -3. Thus, the kernel integral on the triangular dislocation is

$$F_n(\boldsymbol{y}, \theta, p_1, p_2) = \int_\Delta \frac{\mathrm{d}S(\boldsymbol{x})}{[\boldsymbol{h}(p_1)\boldsymbol{x} - \boldsymbol{h}(p_2)\boldsymbol{y}]^n} \quad n = 2,3 \tag{19}$$

where p_1 and p_2 can be assigned to different eigenvalues, according the requirements in Eqs. (13) and (16). In order to carry out the surface integration in Eq. (19) over a triangular dislocation, the following transformation between the global coordinate system (O: x_1, x_2, x_3) and the local coordinate system ($\boldsymbol{x}_0$: ξ_1, ξ_2, ξ_3), associated with the triangular dislocation with the base vectors ξ_i^0 ($i=1$, 2, 3), as shown in Fig. 1, is introduced

$$[\boldsymbol{x} - \boldsymbol{x}_0] = [\mathbf{D}][\xi] \tag{20}$$

where

$$D_{ij} = \boldsymbol{x}_i^0 \cdot \xi_j^0 \tag{21}$$

with $\boldsymbol{x}_0$ being the origin of the local coordinates. Then, the integration in Eq. (19) becomes

$$F_n(\boldsymbol{y}, \theta, p_1, p_2) = \int_\Delta \frac{\mathrm{d}\xi_1 \mathrm{d}\xi_2}{[f_1(\boldsymbol{y}, \theta)\xi_1 + f_2(\boldsymbol{y}, \theta)\xi_2 + f_3(\boldsymbol{y}, \theta)]^n} \quad n = 2,3 \tag{22}$$

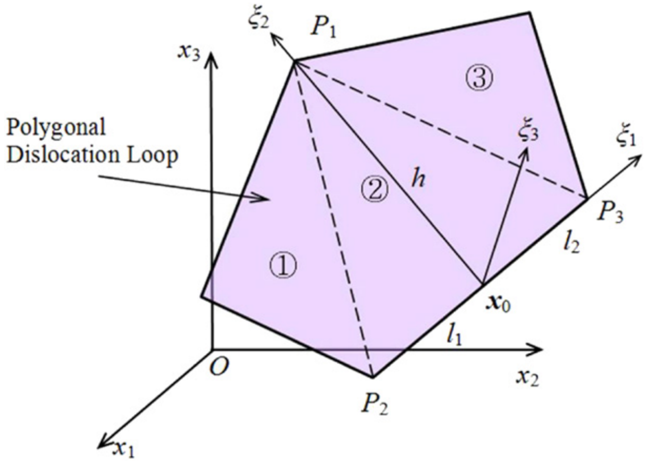

Fig. 1. Geometry of a polygonal dislocation with respect to the global coordinate system (O; x_1, x_2, x_3). This dislocation is divided into three triangles. As an example, a local coordinate system ($\boldsymbol{x}_0$; ξ_1, ξ_2, ξ_3) is attached to the second triangle with its corners P_1, P_2 and P_3, where $h=\xi_2(P_1)$, $l_1=-\xi_1(P_2)$, $l_2=\xi_1(P_3)$. Obviously, l_1 and l_2 can be negative.

where

$$f_\alpha(\boldsymbol{y},\theta,p_1,p_2)=D_{k\alpha}h_k(p_1),\quad \alpha=1,2 \tag{23}$$

$$f_3(\boldsymbol{y},\theta,p_1,p_2)=x_{0k}h_k(p_1)-y_kh_k(p_2) \tag{24}$$

On the triangle $\Delta P_1P_2P_3$ shown in Fig. 1, the integral in Eq. (22) becomes

$$F_n=\int_0^h \mathrm{d}\xi_2\int_{-((h-\xi_2)/h)l_1}^{((h-\xi_2)/h)l_2}\frac{\mathrm{d}\xi_1}{[f_1(\boldsymbol{y},\theta)\xi_1+f_2(\boldsymbol{y},\theta)\xi_2+f_3(\boldsymbol{y},\theta)]^n} \tag{25}$$

By direct integration and with some simplification, we obtain

$$F_2(\boldsymbol{y},\theta,p_1,p_2)=\frac{1}{f_1}\left(\frac{1}{f_2+f_1l_1^*}\ln\frac{f_3^*+f_2}{f_3^*-f_1l_1^*}-\frac{1}{f_2-f_1l_2^*}\ln\frac{f_3^*+f_2}{f_3^*+f_1l_2^*}\right)$$
$$F_3(\boldsymbol{y},\theta,p_1,p_2)=\frac{1}{2}\frac{l_1^*+l_2^*}{h(f_3^*+f_2)(f_3^*+f_1l_2^*)(f_3^*-f_1l_1^*)} \tag{26}$$

with

$$l_1^*=l_1/h,\ l_2^*=l_2/h,\ f_3^*=f_3/h \tag{27}$$

This completes the exact integration of the image displacement Eq. (12) and image strain Eq. (15). The results for the integration over the triangular dislocation loop can be extended to an arbitrarily shaped planar dislocation loop, as shown in the Appendix. The final solution for the displacement and strain fields induced by a triangular dislocation loop contains only line integrals over [0, π] for both the full-space part (Chu et al., 2011) and the image part.

3. Numerical examples

The derived line integrals are employed to calculate the elastic displacements, elastic stresses, and the interaction energy induced by a dislocation loop lying at a prescribed distance from a single aluminum–copper (Al–Cu) bimaterial interface. As Al and Cu are both face-centered cubic (fcc) crystals, a loop in either material can be assumed to lie on a (111) plane with Burgers vector $\boldsymbol{b}=1/2[\bar{1}10]$.

3.1. Displacement and stress fields due to a triangular dislocation

We first consider the solution for a unit triangular loop of arbitrary orientation and check the displacement and traction continuities at the bimaterial interface. As shown in Fig. 2, a regular triangular dislocation with side length a lies in the (111) slip plane, which is located in the upper half-space made of Al ($x_3>0$). The distance from the origin of the local dislocation coordinate system to the Al–Cu interface plane Ox_1x_2 is assumed to be $2a$. Because the solutions' Eqs. (11) and (15) cannot be evaluated exactly at the interface, we calculate the displacements and tractions at five points within a parallel plane above and below the interface plane by $\pm x_3$, where $x_3=10^{-7}$.

The resulting displacements normalized by the magnitude of the Burgers vector $\boldsymbol{b}$ are shown in Table 1 and the tractions or stresses normalized by $\eta\mu$, where $\eta=b/l_{\mathrm{loop}}=b/3a$ and $\mu=\mu(\mathrm{Al})=(C_{1111}-C_{1122}+4C_{2323})_{(\mathrm{Al})}/6$, are given in Table 2. The constant μ is the nominal shear modulus (Hirth and Lothe, 1982). It is clear that the displacement and traction

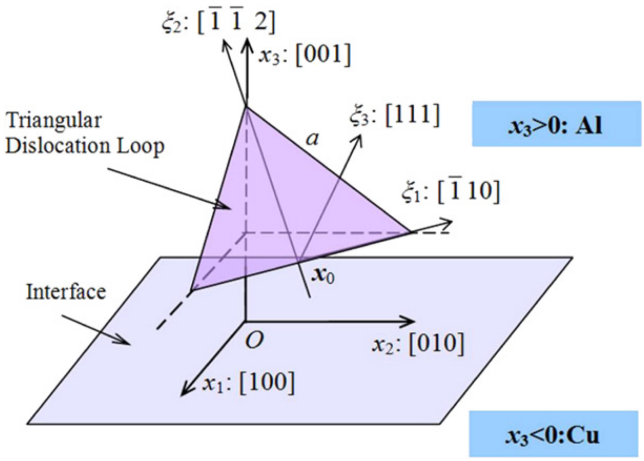

Fig. 2. Geometry of a triangular dislocation in a 3D aluminum–copper bimaterial system, where $x_3>0$ is Al and $x_3<0$ is Cu.

Table 1
Global displacement continuity across the interface $x_3=0$ due to a triangular dislocation in Al of the Al–Cu bimaterials. All displacements are normalized by the magnitude of the Burgers value b.

Points	u_1 $(\times 10^{-3})$	u_2 $(\times 10^{-3})$	u_3 $(\times 10^{-3})$	$\lvert\Delta u_1/\overline{u}_1\rvert$	$\lvert\Delta u_2/\overline{u}_2\rvert$	$\lvert\Delta u_3/\overline{u}_3\rvert$
A^+	0.67164451	-0.67164451	2.7592754×10^{-15}	$<2.3\times10^{-7}$	$<2.3\times10^{-7}$	$<1.0\times10^{-7}$
A^-	0.67164436	-0.67164436	2.7592754×10^{-15}			
B^+	0.76577825	-0.60833022	0.20739566	$<1.8\times10^{-7}$	$<1.3\times10^{-7}$	$<3.0\times10^{-7}$
B^-	0.76577811	-0.60833014	0.20739560			
C^+	1.4396699	-0.47939323	1.8210319	$<2.9\times10^{-7}$	$<2.1\times10^{-7}$	$<3.3\times10^{-7}$
C^-	1.4396695	-0.47939313	1.8210313			
D^+	0.51739796	-1.5798707	-2.0487164	$<2.5\times10^{-7}$	$<3.2\times10^{-7}$	$<2.9\times10^{-7}$
D^-	0.51739783	-1.5798702	-2.0487158			
E^+	0.53924271	-0.50616183	0.16986679	$<2.1\times10^{-7}$	$<2.0\times10^{-7}$	$<2.9\times10^{-7}$
E^-	0.53924260	-0.50616173	0.16986674			

Note: $A^\pm=(0.0, 0.0, \pm x_3)$, $B^\pm=(-0.4, -0.3, \pm x_3)$, $C^\pm=(-0.6, 0.4, \pm x_3)$, $D^\pm=(0.5, -0.7, \pm x_3)$, $E^\pm=(0.3, 0.4, \pm x_3)$ where $x_3=10^{-7}$, Coordinates are all normalized by the side length a of the triangle.

Table 2
Global tractions at the interface ($x_3=0$). All data are normalized by $\eta\mu$(Al).

Points	σ_{13} $(\times 10^{-2})$	σ_{23} $(\times 10^{-2})$	σ_{33} $(\times 10^{-2})$	$\lvert\Delta\sigma_{13}/\overline{\sigma}_{13}\rvert$	$\lvert\Delta\sigma_{23}/\overline{\sigma}_{23}\rvert$	$\lvert\Delta\sigma_{33}/\overline{\sigma}_{33}\rvert$
A^+	-1.25479050	1.254790497	$<1\times10^{-15}$	$<5.6\times10^{-8}$	$<6.4\times10^{-8}$	–
A^-	-1.25479057	1.254790570	$<1\times10^{-15}$			
B^+	-1.22207891	1.560346805	0.544003571	$<8.3\times10^{-8}$	$<1.9\times10^{-8}$	$<3.7\times10^{-7}$
B^-	-1.22207901	1.560346829	0.544003401			
C^+	0.815840579	0.6345267133	4.62601867	$<7.3\times10^{-7}$	$<1.1\times10^{-7}$	$<4.4\times10^{-6}$
C^-	0.815840094	0.6345267859	4.62601723			
D^+	-0.222732960	-1.29575685	-5.04362798	$<9.0\times10^{-7}$	$<4.6\times10^{-7}$	$<4.0\times10^{-7}$
D^-	-0.222733086	-1.29575631	-5.04362653			
E^+	-0.114415563	1.04509261	0.444403217	$<8.7\times10^{-7}$	$<7.7\times10^{-8}$	$<4.5\times10^{-7}$
E^-	-0.114415570	1.04509269	0.444403047			

Note: $A^\pm=(0.0, 0.0, \pm x_3)$, $B^\pm=(-0.4, -0.3, \pm x_3)$, $C^\pm=(-0.6, 0.4, \pm x_3)$, $D^\pm=(0.5, -0.7, \pm x_3)$, $E^\pm=(0.3, 0.4, \pm x_3)$ where $x_3=10^{-7}$, Coordinates are all normalized by the side length a of the triangle.

continuity conditions at the interface are both satisfied with differences being extremely small on both sides of the interface, with a relative error less than 10^{-5}. Also, the displacement jump condition across the dislocation surface should equal the Burgers vector. This condition was satisfied with a maximum relative difference less than 0.4%.

With the method validated, we consider a case in which a dislocation loop in Al approaches a bimaterial interface. Of interest is the effect of this nearby dislocation loop on the displacement and stress distributions across the interface plane. Depending on the properties of the interface, the perturbations in stress caused by the impinging dislocation can, for instance, result in dislocation nucleation in the adjoining Cu or nucleation of interfacial dislocations. In our example, the triangular dislocation is situated symmetrically about $x_2=x_1$. Despite this, we find that neither the individual displacement components u_1 and u_2 nor the distributions of shear stresses σ_{13} and σ_{23} are symmetric about $x_2=x_1$. However, the distribution of $(u_1+u_2)/2$ within the x_2-x_1 interface plane is anti-symmetric and the distribution of $(u_1-u_2)/2$ symmetric, as shown in Fig. 3 and 4, respectively. Likewise, $(\sigma_{13}+\sigma_{23})/2$ (Fig. 5) is anti-symmetric and $(\sigma_{13}-\sigma_{23})/2$ (Fig. 6) is symmetric about $x_2=x_1$. Peak values of these shear displacements and stresses, which are likely regions for nucleating dislocations or voids, are offset from the line of intersection between the dislocation glide plane and the interface plane (see figure captions for peak values).

3.2. The interactive image energy of a hexagonal dislocation loop

The previous section demonstrated how the method developed in this work can be used to study how a dislocation affects the interface. In this section, we investigate the complementary relationship—how an interface perturbs the stress field of a nearby dislocation. In this respect, several factors are studied: the size, orientation, and position of the loop from the interface. The relevance of such details increases as the phase size shrinks, as finer length scales place greater limits on the shape, size, and location of the dislocation loop.

Compared to calculation of the entire stress field, the influence of the bimaterial interface can be revealed more efficiently by studying the variation of the interaction energy contributed by the image stress with d, the distance of the dislocation from the interface. The interaction energy between the bimaterial interface and a dislocation with normal $\mathbf{n}^+$

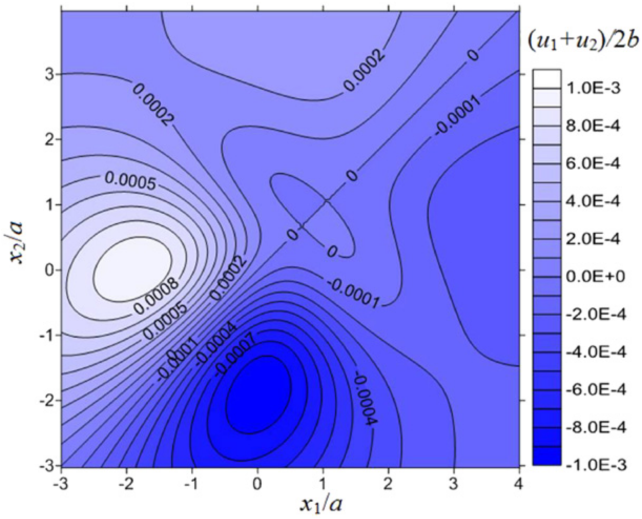

Fig. 3. Distribution of $(u_1+u_2)/2$ normalized by the magnitude of the Burgers vector value b on the interface ($x_3=0$) plane in the global coordinates, where the coordinates are normalized by the side length a of the triangular dislocation. A peak value of 0.00099b is located at point $(-1.81a,0.03a,0)$.

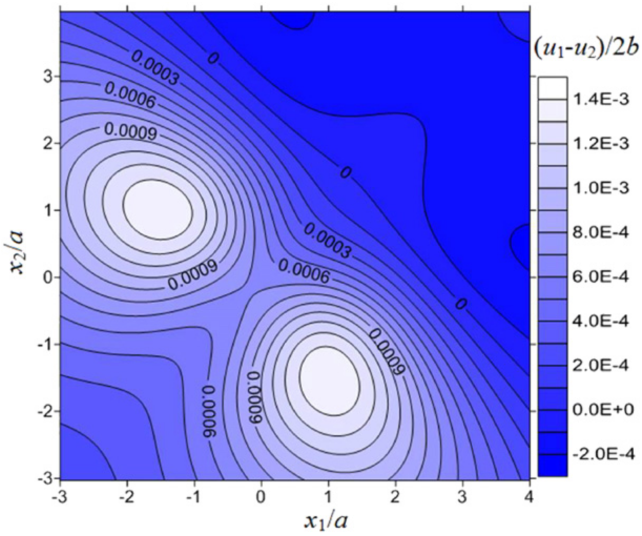

Fig. 4. Distribution of $(u_1-u_2)/2$ normalized by the magnitude of the Burgers vector value b on the interface ($x_3=0$) plane in the global coordinates, where the coordinates are normalized by the side length a of the triangular dislocation. A peak value of 0.0014b is located at point $(-1.52a,1.02a,0)$.

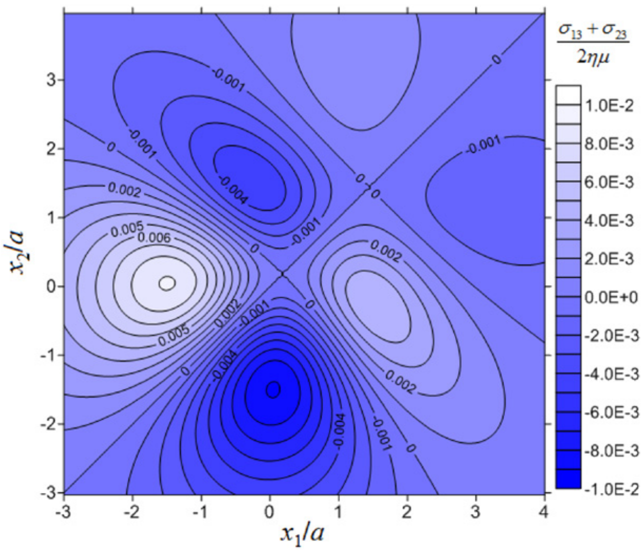

Fig. 5. Distribution of $(\sigma_{13}+\sigma_{23})/2$ normalized by $\eta C_{\max}$ on the interface ($x_3=0$) in the global coordinates, where the coordinates are normalized by a and the normalized peak value is about 0.01.

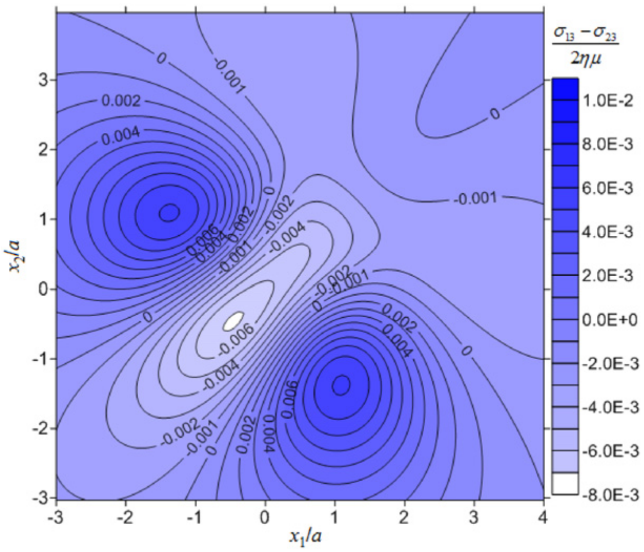

Fig. 6. Distribution of $(\sigma_{13}-\sigma_{23})/2$ normalized by $\eta C_{\max}$ on the interface ($x_3=0$) in the global coordinates, where the coordinates are normalized by a and the normalized peak value is about 0.01. The maximum normalized shear stresses σ_{13} and σ_{23} are equal but reached at different points.

and Burgers vector **b** can be calculated using (Hirth and Lothe, 1982),

$$E=\frac{1}{2}\int_S \sigma^+\mathbf{n}^+\,\mathrm{d}s\mathbf{b} \tag{28}$$

For a bimaterial system, E is the sum of the energetic contributions from the full-space stress, denoted by E^{Full}, and from the image stress, denoted by E^{Image}. The change in energy ΔE due to a change in d can be attributed only to the change in the image stress and not the homogeneous stress in the full space, i.e., $\Delta E=\Delta E^{\mathrm{Image}}$. For a straight dislocation in a bimaterial system, the relationship between the image energy and d was found to be $\Delta E=-A\ln(d)$ (Barnett and Lothe, 1974).

In this example, we also consider a hexagonal dislocation loop. This loop geometry is built from several unit triangles, and hence demonstrates the superposition method as well. The present method calculates the image stress for a hexagonal dislocation loop that is then substituted into Eq. (28) for the image energy E^{Image}. We also consider two typical situations: (a) one in which the glide plane is inclined to the interface plane, and (b) the other in which the glide plane is parallel to the interface plane, as shown in Fig. 7a and b. For convenience in describing the dependence of the image energy on d, the dimensionless quantity $E^{\mathrm{Image}}/\mu b^2 l_{\mathrm{loop}}$ is defined where $\mu=\mu(\mathrm{Al})$ if the dislocation loop is in Al or $\mu=\mu(\mathrm{Cu})$ if the dislocation loop is in Cu, and $l_{\mathrm{loop}}=6a$.

For the inclined case, the resulting variation of E^{Image} with d is shown in Fig. 8. Because Cu has a larger shear stiffness than Al, $\mu(\mathrm{Cu})>\mu(\mathrm{Al})$, E^{Image} is positive when the dislocation is in Al and negative when the dislocation is in Cu.

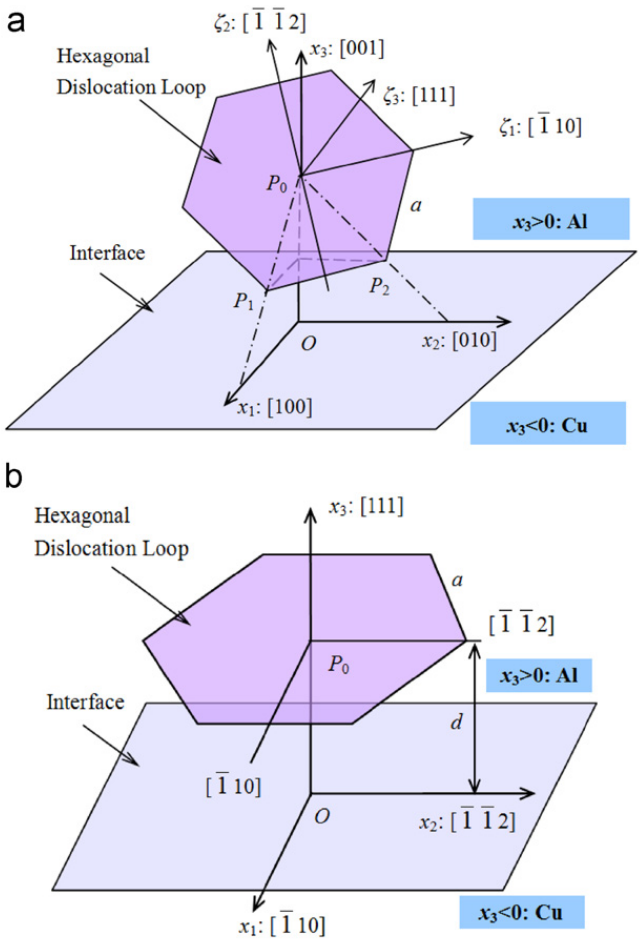

Fig. 7. Geometry of a hexagonal dislocation in the aluminum–copper bimaterials: (a) the dislocation plane is inclined to the interface, and (b) the dislocation plane is parallel to the interface. The dislocation is located in the upper half space (Al) with its central distance to the interface being d. The lower layer is Cu.

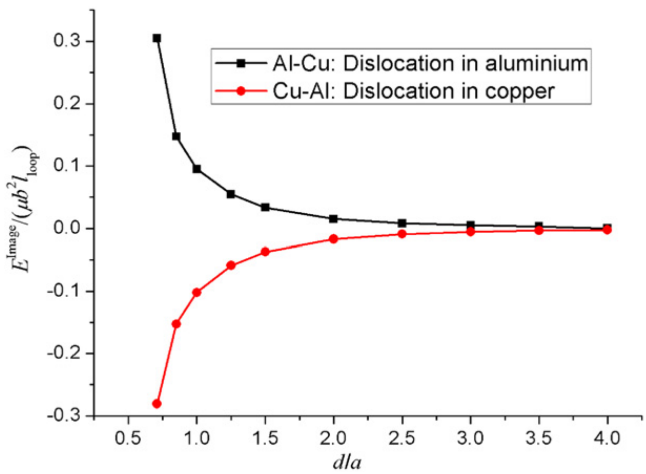

Fig. 8. The influence of the position of a hexagonal dislocation on the interactive image energy E^{Image} in bimaterials, where d is the distance between the center of the dislocation and bimaterial interface, and a is the side length of the dislocation.

The decrease in E^{Image} as the distance d increases can be well described by a power law,

$$\frac{E^{\text{Image}}}{\mu b^2 l_{\text{loop}}} = A\left(\frac{d}{a}\right)^m \tag{29}$$

where A and m are constants that depend on the elastic moduli mismatch, and the shape, size, and orientation of the dislocation loop. For the dislocation in Al, $A=0.0954$ and $m=-3.33$; and for the dislocation in Cu, $A=-0.103$ and

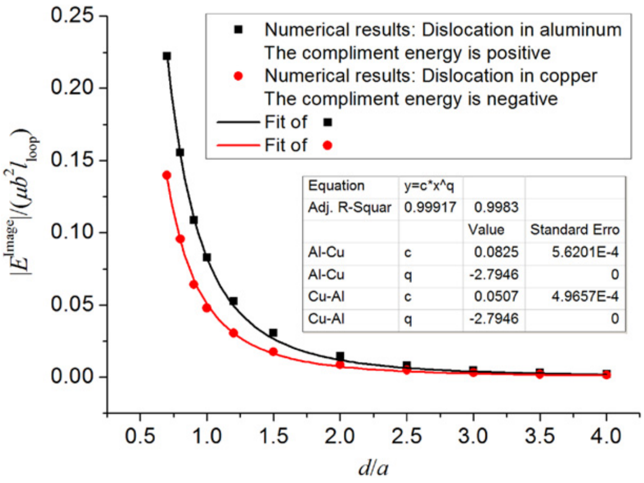

Fig. 9. The size effect of a hexagonal dislocation on the interactive image energy E^{Image} where the dislocation loop is parallel to the interface plane and a is the side length of the hexagonal dislocation.

$m=-2.88$. Obviously, compared to the logarithmic decay for a 2D dislocation, the energy for a 3D dislocation decays more rapidly as the dislocation moves away from the interface.

For the parallel case, the variation in E^{Image} with the distance d and the size is shown in Fig. 9, clearly showing the size and distance effect of a hexagonal dislocation on the complement energy. Similar to the previous result for the oblique dislocation case, the energy decreases rapidly with the increase in d. However, the effect of the size (a) and the distance (d) can be decoupled due to the geometry. Again, it is found that the image energy can be described well by the following power-law relationship:

$$\frac{|E^{\text{Image}}|}{\mu b^2 l_{\text{loop}}}=C\left(\frac{d}{a}\right)^q \tag{30}$$

where $\mu=\mu(\text{Al})$, and C and q are parameters given in the inset table in Fig. 9. A remarkable feature in Eq. (30) is that the power-order parameter q is the same no matter if the dislocation lies in Al or Cu. As a result, one thus finds from Eq. (29) and (30) that

$$\frac{E_1^{\text{Image}}}{E_2^{\text{Image}}}=\frac{a_1}{a_2}=\frac{d_2}{d_1} \tag{31}$$

for a dislocation loop in the same material when the ratio d/a is fixed. The subscripts denote two different loop sizes and distances from the interface in the same material. This simple relation clearly shows that only two geometric parameters, d and a, affect the image energy for a hexagonal dislocation lying parallel to the interface plane and more importantly, this energy only depends on their ratio d/a. The validity of Eq. (31) is confirmed by testing numerically several cases in which $d/a=1$, 2. For the example of $d/a=2$, the image energies for different d and a ($d=3a_0$, $a=1.5a_0$), ($d=1.5a_0$, $a=0.75a_0$) and ($d=2a_0$, $a=a_0$), differ less than 10^{-4}.

We further analyze the image interaction energy of a hexagonal dislocation in a hypothetical bimaterial system where the Al crystal is bound to a tunable material B in the lower half space. In this way, the influence of the elastic moduli mismatch can be systematically studied. Specifically the elastic modulus of B is defined as $C_{ijkl}(B)=\alpha C_{ijkl}(\text{Al})$, where α is a tunable coefficient. Fig. 10 shows the variation of the image energy with $\ln(\alpha)$ for a dislocation loop on an inclined glide plane (Fig. 7a). For three different ratios $d/a=1.0$, 1.5, and 2.0, the results show that the three curves in Fig. 10 intersect at $\ln(\alpha)=0$, where the elastic stiffness for material B and Al are identical, corresponding to the zero image energy. In addition, the image energy increases with increasing α (or the stiffness of $C_{ijkl}(B)$). Significantly when α is in the range of 0.1 to 10, the image energy E^{Image} and the coefficient α approximately follow the logarithmic relationship shown in the insert in Fig. 10, i.e.,

$$\frac{E^{\text{Image}}}{\mu b^2 l_{\text{loop}}}=D\ln(\alpha) \tag{32}$$

where D is a constant. In this example, $D=0.127$ for $d/a=1.0$, 0.0463 for $d/a=1.5$ and 0.0215 for $d/a=2.0$. It is also noted that the variation in the image energy with α shows three interesting features as described by three regimes: For α less than 10, the image energy obeys the logarithmic relationship with α given in Eq. (32). For α in the range from 10 to 50, the image energy increases at a slower rate than that in Eq. (32), e.g., the net increase is about $\sim$18% as α increases from 10 to 50. However, for $\alpha>50$, the image energy is virtually insensitive to the elastic moduli mismatch. The increase is about 4.0% as α increases from 50 to 1000, which represents a soft material bounded to a rigid one. This is one of our main results, that the interactive image energy only depends on d/a, a finding that will benefit development of simplified models for dislocation-interface interactions, ones that are more amenable for implementation into higher length scale models of interface-driven plasticity.

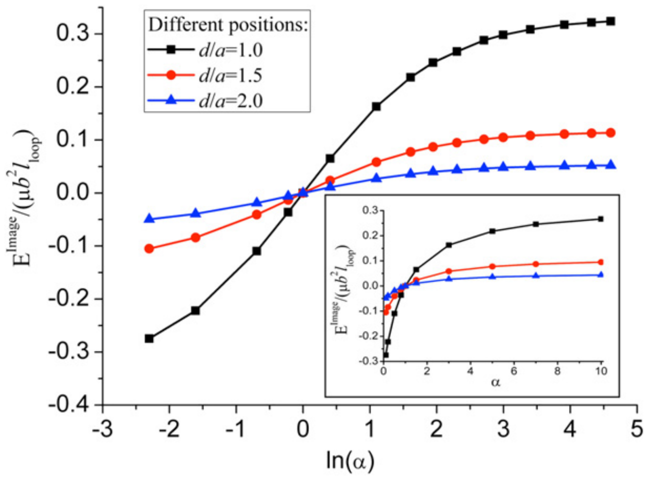

Fig. 10. The influence of interface elastic moduli mismatch on the interaction image energy E^{Image}. The insert represents the variation when $\alpha=0.1\sim10$. d is the distance between the center of the hexagonal dislocation and the bimaterial interface, and a is the side length of the hexagonal dislocation.

4. Conclusions

In this work, we have derived line integral expressions (from 0 to π) for the elastic displacement and strain (stress) fields due to an arbitrary polygonal dislocation in the 3D anisotropic bimaterial system. In our formulation, the standard triple integral expression is reduced to the simple line integral, making it convenient for studying dislocations with arbitrary arrangement in the two-material system. In the present examples we study the displacement and stress fields generated by a dislocation loop in an aluminum–copper bimaterial system. We also calculate the variation in the interactive image energy for a dislocation loop of different sizes approaching the interface from either a soft or stiff material. We find that the interactive image energy for a dislocation loop decays according to a power-law relationship, much faster than a straight dislocation. Significantly, we reveal that the interactive image energy depends only on the ratio d/a, where a is the loop diameter and d is its distance to the interface. We further demonstrate how to extract the power–law relationship with pre-factors determined by the present calculation, which is useful in transition of the results of this work to higher length scale models involving several arrays of dislocations interacting with a bimaterial interface.

This powerful technique can also be applied to model several dislocation loops of arbitrary arrangement interacting with a bimaterial interface. The next steps are to extend this technique to multilayers, where the effect of relative layer thickness on the elastic fields can be explored, and to account for atomic-scale information such as the elastic fields contributed by the atomic-scale lattice mismatch across the interface or interactions with interfacial dislocations.

Acknowledgments

H. Chu acknowledgments the financial support provided by the National Natural Science Foundation (10602050) and a Jiangsu Government Scholarship for overseas studies. H. Chu, J. Wang and I.J. Beyerlein acknowledge support provided by Los Alamos National Laboratory Directed Research and Development (LDRD) project DR20110029. J. Wang also acknowledges support provided by the U.S. Department of Energy, Office of Science, Office of Basic Energy Sciences and a Los Alamos National Laboratory Directed Research and Development (LDRD) project ER20110573. X. Han was supported by National Natural Science Foundation (10672021). The authors are very grateful to both reviewers for their valuable and constructive comments and suggestions. The derivation in the appendix is own to Prof. Robert V. Kukta at State University of New York at Stony Brook, who would like to share it to the dislocation community.

Appendix A

To extend the integral of Eq. (22) over a triangle loop to the integral over an arbitrarily shaped planar loop S, as suggested by one of the reviewers on this article, one may redefine

$$F_n=\int_S \frac{\mathrm{d}\xi_1\mathrm{d}\xi_2}{[f_1\xi_1+f_2\xi_2+f_3]^n} \tag{A.1}$$

Letting

$$L_n(\xi_1,\xi_2)=\int_{-\infty}^{\xi_1}\frac{\mathrm{d}\xi_1}{(f_1\xi_1+f_2\xi_2+f_3)^n} \tag{A.2}$$

one has

$$\frac{\partial L_n(\xi_1,\xi_2)}{\partial \xi_1} = \frac{1}{(f_1\xi_1+f_2\xi_2+f_3)^n} \tag{A.3}$$

Substituting Eq. (A.3) to (A.1), one gets

$$F_n = \int_S \frac{\partial L_n(\xi_1,\xi_2)}{\partial \xi_1} \mathrm{d}\xi_1 \mathrm{d}\xi_2 = \int_{\partial S} L_n(\xi_1,\xi_2)\mathrm{d}\xi_2 \tag{A.4}$$

Thus, the surface integral over the dislocation slip plane is translated into the line integral along the dislocation line. It is noted that on the dislocation boundary ∂S, $\xi_1 = \xi_1(\xi_2)$. For a straight line segment from point$(\xi_1,\xi_2) = (a_1,a_2)$ to point $(\xi_1,\xi_2) = (b_1,b_2)$, one finds

$$F_2^{\text{segment}} = \frac{a_2-b_2}{f_1[(a_1-b_1)f_1+(a_2-b_2)f_1]} \ln\left(\frac{b_1f_1+b_2f_2+f_3}{a_1f_1+a_2f_2+f_3}\right) \tag{A.5}$$

Applying Eq. (A.5) to the triangle used in Eq. (22), we find the same integral results given in the first expression in Eq. (26). It is noted that Eq. (A.4) is valid for an arbitrary planar dislocation loop, including the polygonal loop as its special case.

References

Akasheh, F., Zbib, H.M., Hirth, J.P., Hoagland, R.G., Misra, A., 2007a. Dislocation dynamics analysis of dislocation intersections in nanoscale metallic multilayered composites. J. Appl. Phys. 101, 084314.

Akasheh, F., Zbib, H.M., Hirth, J.P., Hoagland, R.G., Misra, A., 2007b. Interactions between glide dislocations and parallel interfacial dislocations in nanoscale strained layers. J. Appl. Phys. 102, 034314.

Akarapu, S., Zbib, H.M., 2009. Line-integral solution for the stress and displacement fields of an arbitrary dislocation segment in isotropic bi-materials in 3D space. Phil. Mag. 89, 2149–2166.

Anderson, P.M., Foecke, T., Hazzledine, P.M., 1999. Dislocation-based deformation mechanisms in metallic nanolaminates. MRS Bull. 24, 27–33.

Barnett, D.M., Lothe, J., 1974. An image force theorem for dislocations in bicrystals. J. Phys. F 4, 1618–1635.

Ben-Zion, Y., 1990. The response of two half spaces to point dislocations at the material interface. Geophys. J. Int. 101, 507–528.

Cai, W., Arsenlis, A., Weinberger, C.R., Bulatov, V.V., 2006. A non-singular continuum theory of dislocations. J. Mech. Phys. Solids 54, 561–587.

Chu, H.J., Pan, E., Wang, J., Beyerlein, I.J., 2011. Three-dimensional elastic displacements induced by a dislocation of polygonal shape in anisotropic elastic crystals. Int. J. Solids Struct. 48, 1164–1170.

Chu, H.J., Wang, J., Zhou, C.Z., Beyerlein, I.J., 2011. Self-energy of elliptical dislocation loops in anisotropic crystals and its application for defect-free core/shell nanowires. Acta Mater. 59, 7114–7124.

Comninou, M., Dundurs, J., 1975. The angular dislocation in a half Space. J. Elasticity 5, 203–216.

Demkowicz, M.J., Wang, J., Hoagland, R.G., 2008. Interfaces between dissimilar crystalline solids. In: Hirth, J.P. (Ed.), Dislocations in Solids, vol. 14. North-Holland. Chap. 83, pp. 141–207.

Fares, N., Li, V.C., 1988. General image method in a plane-layered elastostatic medium. J. Appl. Mech. 55, 781–785.

Fitzgerald, S.P., Aubry, S., 2010. Self-force on dislocation segments in anisotropic crystals. J. Phys.: Condens. Matter 22, 295403.

Freund, L.B., 1990. The driving force for glide of a threading dislocation in a strained epitaxial layer on a substrate. J. Mech. Phys. Solids 38, 657–679.

Gavazza, S.D., Barnett, D.M., 1976. The self-force on a planar dislocation loop in an anisotropic linear-elastic medium. J. Mech. Phys. Solids 24, 171–185.

Ghoniem, N.M., Han, X., 2005. Dislocation motion in anisotropic multilayer materials. Phil. Mag. 85, 2809–2830.

Gosling, T.J., Willis, J.R., 1994. A line-integral representation for the stresses due to an arbitrary dislocation in an isotropic half-space. J. Mech. Phys. Solids 42, 1199–1221.

Han, W.Z., Carpenter, J.S., Wang, J., Beyerlein, I.J., Mara, N.A., 2011. Atomic-level study of twin nucleation from fcc/bcc interfaces in nanolamellar composites. Appl. Phys. Lett., in preparation.

Han, X., Ghoniem, N.M., 2005. Stress field and interaction forces of dislocations in anisotropic multilayer thin films. Phil. Mag. 85, 1205–1225.

Hirth, J.P., Lothe, J., 1982. Theory of Dislocations, 2nd ed. John &Willy Publisher.

Lu, K., Lu, L., Suresh, S., 2009. Strengthening materials by engineering coherent internal boundaries at the nanoscale. Science 324, 349–352.

Mara, N.A., Bhattacharyya, D., Dickerson, P., Hoagland, R.G., Misra, A., 2008. Deformability of ultrahigh strength 5nm Cu/Nb nanolayered composites. Appl. Phys. Lett. 92, 231901.

Mara, N.A., Bhattacharyya, D., Hirth, J.P., Dickerson, P., Misra, A., 2010. Mechanism for shear banding in nanolayered composites. Appl. Phys. Lett. 97, 021909.

Mindlin, R.D., 1936. Force at a point in the interior of a semi-infinite solid. Physics 7, 195–202.

Misra, A., Verdier, M., Kung, H., Embury, J.D., Hirth, J.P., 1999. Deformation mechanism maps for polycrystalline metallic multiplayers. Scripta Mater. 41, 973.

Misra, A., Kung, H., 2001. Deformation behavior of nanostructured metallic multilayers. Adv. Eng. Mater. 3, 217.

Misra, A., Hirth, J.P., Kung, H., 2002. Single-dislocation-based strengthening mechanisms in nanoscale metallic multilayers. Phil. Mag. 82, 2935.

Misra, A., 2008. Twinning in nanocrystalline metals. JOM 60, 59.

Mura, T., 1963. Continuous distribution of moving dislocations. Phil. Mag. 8, 843–857.

Mura, T., 1987. Micromechanics and Defects in Solids, 2nd ed. Martinus Nijho.

Pan, E., 1991. Dislocation in an infinite poroelastic medium. Acta Mech. 87, 105–115.

Pan, E., Yuan, F.G., 2000. Three-dimensional Green's functions in anisotropic bimaterials. Int. J. Solids Struct. 37, 5329–5351.

Ting, T.C.T., 1996. Anisotropic Elasticity: Theory and Applications. Oxford University Press, New York.

Tonon, F., Pan, E., Amadei, B., 2001. Green's functions and boundary element method formulation for 3D anisotropic media. Comput. Struct. 79, 469–482.

Volterra, V., 1907. Sur l'équilibre des corps élastiques miltiplement connexes. Annis EC. Norm. Sup. 24, 401–517.

Wang, C.Y., 1996. The stress field of a dislocation loop in an anisotropic solid. J. Mech. Phys. Solids 44, 293–305.

Wang, J., Hoagland, R.G., Hirth, J.P., Misra, A., 2008a. Atomistic simulations of the shear strength and sliding mechanisms of copper–niobium interfaces. Acta Mater. 56, 3109–3119.

Wang, J., Hoagland, R.G., Hirth, J.P., Misra, A., 2008b. Atomistic modeling of the interaction of glide dislocations with weak interfaces. Acta Mater. 56, 5685–5693.

Wang, J., Hoagland, R.H., Hirth, J.P., Misra, A., 2009a. Room-temperature dislocation climb in metallic interfaces. Appl. Phys. Lett. 94, 131910.

Wang, J., Hoagland, R.G., Misra, A., 2009b. Mechanics of nanoscale metallic multilayers: From atomic-scale to micro-scale. Scripta Mater. 60, 1067–1072.

Wang, J., Misra, A., 2011. An overview of interface-dominated deformation mechanisms in metallic multilayers. Curr. Opinion Solid State Mater. Sci. 15, 20–28.
Wang, J., Misa, A., Hoagland, R., Hirth, J.P. 2011. Slip transmission across fcc/bcc interfaces with varying interface shear strength. Acta Mater. (in press).
Willis, J.R., 1970. Stress fields produced by dislocations in anisotropic media. Phil. Mag. 21, 931–949.
Yu, H.Y., Sanday, S.C., 1991. Circular dislocation loops in bimaterials. J. Phys.: Condens. Matter 3, 3081–3090.
Zhang, R.F., Wang, J., Beyerlein, I.J., Germann, T.C., 2011. Dislocation nucleation mechanisms from fcc/bcc incoherent interfaces. Scripta Mater. 65, 1022–1025.